

## Original Article



## Photothermal Effect-based Cytotoxic Ability of Melanin from *Mytilus edulis* Shells to Heal Wounds Infected with Drug-resistant Bacteria *in vivo*\*

LIU Ya Mei<sup>1</sup>, MA Wei Shuai<sup>1</sup>, WEI Yu Xi<sup>1</sup>, and XU Yuan Hong<sup>1,2,#</sup>

1. Institute of Biomedical Engineering, College of Life Sciences, Qingdao University, Qingdao 266071, Shandong, China; 2. Department of Urology, Key Laboratory of Urinary System Diseases, The Affiliated Hospital of Qingdao University, Qingdao 266003, Shandong, China

### Abstract

**Objective** Owing to antibiotic abuse and the subsequent development of antibiotic resistance, bacterial infection has become one of the most persistent unresolved problems. New antibacterial agents, especially those that are environmental-friendly, are urgently needed.

**Methods** Melanin extracted by filtration centrifugation and acid and proteolytic hydrolysis was characterized using UV, FTIR, TEM, and XPS. Photothermal conversion was calculated, and the bacteriostatic effects, *in vitro* and *in vivo*, were assessed by plate counting and ratios (%) of wound areas.

**Results** Natural melanin hydrolyzed by trypsin had good photothermal conversion effects, which resulted in superior bacteriostatic activities. The extracted melanin along with laser NIR irradiation at 808 nm promoted the healing of wounds infected by drug-resistant bacteria *in vivo* and was biocompatible according to toxicity tests *in vivo* and *in vitro*.

**Conclusion** The present findings indicated a safe and efficient method of developing natural antibacterial agents.

**Key words:** Melanin; Photothermal conversion; Antibacterial; Wound healing

*Biomed Environ Sci*, 2020; 33(7): 471-483 doi: 10.3967/bes2020.052

ISSN: 0895-3988

[www.besjournal.com](http://www.besjournal.com) (full text)

CN: 11-2816/Q

Copyright ©2020 by China CDC

### INTRODUCTION

Bacterial infections occur during most wound repair processes after exposure to tissue damage, and severe inflammatory reactions often delay wound healing<sup>[1,2]</sup>. Bacterial infections kill tens of thousands of people worldwide annually<sup>[3]</sup>, and this has incited considerable panic, particularly because of antibiotic resistance<sup>[4]</sup>.

Various materials with antibacterial properties, including biocides, metal ions<sup>[5]</sup>, carbon nanotubes<sup>[6]</sup>, quaternary ammonium compounds<sup>[7]</sup>, noble metal materials<sup>[5]</sup>, and metal oxide nanoparticles<sup>[8]</sup>, have been established to date. However, all of these antibacterial materials are chemically synthesized and thus have some inadequacies, such as complex preparation processes, high costs, biotoxicity, and/or possible environmental pollution<sup>[9]</sup>. Safe, effective,

\*This study was supported by the National Natural Science Foundation of China [No. 21874079]; Nature Science Foundation for Outstanding Young Scientists of Shandong Province [No. ZR2018JL011]; Key R & D Project of Shandong Province [No. GG201809230180]; Taishan Scholars Program of Shandong Province [No. tsqn201909088]; Outstanding Youth Innovation Team of Universities in Shandong Province [No. 2019KJA027]; Science & Technology Fund Planning Project of Shandong Colleges and Universities [No. J16LA13 & J18KA112].

#Correspondence should be addressed to XU Yuan Hong, Tel: 86-15264285082, E-mail: yhxu@qdu.edu.cn

Biographical note of the first author: LIU Ya Mei, female, born in 1995, Master's Degree, majoring in high value utilization of marine resources.

and environmental-friendly antibacterial agents are urgently needed to combat bacterial infections and accelerate wound healing<sup>[10-13]</sup>.

Photothermal treatment has become an alternative option for treating some types of bacterial infections<sup>[14,15]</sup>. It is associated with the integration of an appropriate energy absorber within locoregional tissues. Therein, a near-infrared laser causes therapeutic local hyperthermia and the subsequent death of surrounding malignant cells<sup>[16]</sup>. Carbon and nanoparticles of various metals such as V, Mn, Ce, and Pt, have been developed; however, their dismal metabolism finally results in toxicity and harmful health effects, including changes in mitochondrial respiration, immune responses, and genetic toxicity<sup>[17]</sup>.

Melanin is a polyphenolic compound with an anthracene ring as its monomer unit<sup>[18]</sup>. Melanin is the cause of brown, black, and gray coloration in plants, microorganisms, and animals, as well as in the skin, hair, and eyes of humans<sup>[19]</sup>. Synthetic polydopamine melanin nanoparticles are an alternative to photothermal treatment because of their high energy absorption capacity after laser irradiation. The absorption efficiency of these melanin nanoparticles is high in the infrared region, the energy has a high conversion rate to heat, and they are significantly stable against irradiation<sup>[20]</sup>. Naturally-derived melanin should have good biocompatibility and biostability, because it does not elicit side effects including cytotoxicity and antigen responses *in vitro*<sup>[21-23]</sup> or when injected into organisms *in vivo*<sup>[20]</sup>. Natural melanin has been investigated for over half a century now, and recent studies have also targeted melanin from cuttlefish<sup>[24,25]</sup> and squid<sup>[26,27]</sup>. Melanin has poor solubility because it is usually combined with proteins and polysaccharide, from which it is difficult to separate, and experts have not yet been able to define its structure<sup>[28-30]</sup>. Thus, naturally sourced melanin needs to be explored in detail. Mussel shells contain natural melanin. The meat of the blue mussel, *Mytilus edulis* (*M. edulis*), is delicious and it has a high protein content; hence, these mollusks have been described as 'the eggs of the sea'. However, recent studies on *M. edulis* have focused mainly on its edible parts<sup>[31-33]</sup>, as a result, a large number of *M. edulis* shells were discarded because they cannot be used reasonably. If melanin is extracted from *M. edulis* shells, it can not only broaden the source of melanin, but also reduce the environmental pollution of waste mussel shells. Therefore, more studies on *M. edulis* melanin are

needed from the viewpoints of protecting the environment, comprehensive utilization of natural resources, and biological therapies.

Here, we characterized and assessed the bacteriostatic properties of melanin extracted from *M. edulis*. We then investigated its ability to promote the healing of wounds infected with drug-resistant bacteria and its biological toxicity *in vitro* and *in vivo*.

## MATERIALS AND METHODS

Shells of *M. edulis* were obtained from the coast near Rizhao in Shandong province. We purchased 12 mol/L HCl, NaOH, pepsin, trypsin, neutral protease, alkaline protease, complex protease and animal protease from Sinopharm Chemical Reagent Co. Ltd. (Shanghai, China). The source of Luria-Bertani (LB) medium, propidium iodide (PI), and 4'-6-diamidino-2-phenylindole (DAPI) was Thermo Fisher Scientific Inc. (Waltham, MA, USA) and 3-(4,5-dimethyl-2-thiazolyl)-2,5-diphenyltetrazolium bromide (MTT) was from Sigma-Aldrich Corp., (St. Louis, MO, USA). *Escherichia coli* producing extended-spectrum  $\beta$ -lactamase (ESBL) and methicillin-resistant *Staphylococcus aureus* (MRSA), were provided by the Biology Experimental Teaching Centre of Qingdao University. Mouse fibroblasts (L929) and human umbilical vein endothelial cells (HUVEC), were provided by the Affiliated Hospital of Qingdao University. All reagents used in this study were analytical grade and applied without further purification. The Institutional Animal Care and Use Committee (IACUC) at Qingdao University approved all the experimental protocols. Ultrapure 18.2 M $\Omega$  water was obtained from Millipore Sigma Co., Ltd., Burlington, MA, USA).

### Apparatus

Shells of *M. edulis* were crushed using a DXF-10A High-speed pulverizer (Guangzhou Duoshun Machinery Co. Ltd., Guangzhou City, China). A JEM-2100 transmission electron microscopy (TEM) microscope was obtained from JEOL Ltd. (Tokyo, Japan). Infrared spectra were acquired using a Nicolet Nexus470 infrared spectrometer (Thermo Fisher Scientific Inc.). X-ray photoelectrons (XPS) were measured using a PHI 5000 Versaprobe-II spectrometer (Sigmatech Inc., Huntsville AL, USA) and a monochromatic Al K $\alpha$  (1486.6 eV) source. Photothermal radiation was applied using a near infrared laser transmitter (Shenzhen Shenan Medical Device Factory, Shenzhen, China). Images were

acquired using an S-4800 scanning electron microscope (SEM) (Hitachi Ltd., Tokyo, Japan). Fluorescence images were assessed using a TCS SP8 CARS fluorescence confocal microscope (Leica Cameras AG., Wetzlar, Germany). All samples were refrigerated at  $-80\text{ }^{\circ}\text{C}$  (Qingdao Haier Special Electric Freezer Co. Ltd., Qingdao, China).

### Methods

**Extraction Procedures** Washed, dried and powdered *M. edulis* shells were mixed with 4 mol/L HCl, and filtered to remove remaining  $\text{CaCO}_3$ . The filtrate was mixed with 1 mol/L NaOH and separated by  $1,880\times g$  centrifugation (Anting Scientific Instrument Factory, Shanghai, China). The pH of the supernatant was adjusted to 1.5, to obtain a precipitate that was sedimented by centrifugation and washed several times with distilled water to obtain a crude melanin product. This product was hydrolyzed with HCl (H-melanin) and trypsin (T-melanin) under appropriate conditions, and dried. Supplementary Information shows experimental details.

### Characterization of H-melanin and T-melanin

Hydrolyzed melanin was assessed using ultraviolet spectrophotometry. Functional groups were identified, and the structures of H-melanin and T-melanin were determined using Fourier transform infrared spectroscopy (FTIR). Their internal structures were characterized using SEM and X-ray photoelectron spectroscopy (XPS)<sup>[34]</sup>. Supplementary Information contains more experimental details.

### Determination of Photothermal Conversion

Hydrolyzed melanin (13 mg) samples were placed in EP tubes, irradiated at 0.8 W and 808 nm with a near-infrared laser for 7 min, then temperature was recorded every minute to compare the photothermal conversion capability of H-melanin and T-melanin. The samples were treated with water dispersion at 25–200  $\mu\text{g}/\text{mL}$  then laser-irradiated at  $2\text{ W}/\text{cm}^2$  and 808 nm for 5 min with pure deionized water as the negative control.

**Antibacterial Activity in vitro** Single colonies of resistant *Staphylococcus aureus* (*S. aureus*) and *Escherichia coli* (*E. coli*) were inoculated onto solid LB medium and into 50 mL of sterile liquid LB medium (containing tryptone 0.5 g, yeast extract 0.25 g and NaCl 0.5 g) and agitated overnight at  $180\text{ rev min}^{-1}$  in a rotary shaker at  $37\text{ }^{\circ}\text{C}$ . Thereafter, the bacterial suspensions were diluted in sterile phosphate buffered saline (PBS) to a density of  $1\times 10^6$  colony forming units (CFU)/mL<sup>[35,36]</sup>. Hydrolyzed melanin (20  $\mu\text{L}$ ; 2  $\text{mg}/\text{mL}$ ) suspended in sterile water was

mixed with 200  $\mu\text{L}$  of bacterial suspensions. Blank controls contained PBS instead of melanin. The bacterial samples were exposed or not to near infrared radiation (NIR; 2 W, 808 nm, power density  $8\text{ W}/\text{cm}^2$ , continuous output) for 15 min with shaking every 5 min. Thereafter, the samples were shaken for 30 min at  $37\text{ }^{\circ}\text{C}$ , then 200  $\mu\text{L}$  was evenly streaked onto plates containing LB medium and left for 24 h at  $37\text{ }^{\circ}\text{C}$ . CFU were counted<sup>[37]</sup> and the bacteria were characterized using TEM<sup>[38,39]</sup>.

Suspensions of aqueous H-melanin and T-melanin (50  $\mu\text{L}$ ; 20  $\text{mg}/\text{mL}$ ) added to 500  $\mu\text{L}$  of fresh *E. coli* and *S. aureus* suspensions were shaken, then and irradiated or not with NIR (2W, 808 nm) for 15 min. The blank control contained PBS, and was incubated at  $37\text{ }^{\circ}\text{C}$  for 30 min. The bacterial suspensions were mixed with 500  $\mu\text{L}$  of sterile water, then separated by centrifugation at 8,000 rpm. The precipitate was resuspended in 500  $\mu\text{L}$  of water<sup>[40]</sup>, stained with 200  $\mu\text{L}$  DAPI (12.5  $\mu\text{g}/\text{mL}$ ) and PI (1.25  $\mu\text{g}/\text{mL}$ ) for 15 min and left at room temperature in darkness for 30 min. The stained samples were then assessed by fluorescence microscopy.

**Wound Healing in vivo** The ability of hydrolyzed melanin to heal wounds was evaluated in 6-week-old Sprague-Dawley rats weighing 200 g. Round wounds with a diameter of 6 mm prepared on the backs of the rats, and infected with 20  $\mu\text{L}$  *S. aureus* ( $10^6$  CFU/mL). The wounds were then treated with PBS, H-melanin or T-melanin, and with or without NIR irradiation for 15 mins. The wounds were photographed daily. Rats were sacrificed on days 0, 3, and 6 to collect wound tissues, and skin covering entire wounds and normal adjacent skin were extracted and incubated at  $37\text{ }^{\circ}\text{C}$  in LB liquid medium overnight. Thereafter, CFU were counted.

Wound tissues collected on days 3 and 6 were fixed in 4% paraformaldehyde, embedded in paraffin, sliced into 4- $\mu\text{m}$  sections, and stained with hematoxylin and eosin (H&E) for histological assessment<sup>[41]</sup>.

### Cytotoxicity and Biocompatibility in vitro and in vivo

The cytotoxicity of hydrolyzed melanin was assessed in HUVEC and L929 cells *in vitro* using MTT assays.

The biosafety of melanin was also assessed *in vivo*. Rats were intravenously injected with PBS (control), or H-melanin and T-melanin (200  $\mu\text{g}/\text{mL}$ ). The rats were euthanized 6 days later, and the liver, heart, spleen, lungs, and kidneys were harvested. Blood was also collected from those injected with melanin to examine physiological

indexes.

## RESULTS AND DISCUSSION

### Characterization of Melanin Hydrolyzed with HCl and with Trypsin

The ultraviolet spectra of melanin extracted from *M. edulis* shells were characterized. A maximum absorption peak near 230 nm (Supplementary Figure S1A, available in [www.besjournal.com](http://www.besjournal.com)), and the black color of the shell extracts indicated that the extract was melanin<sup>[42,43]</sup>.

We further examined whether the hydrolyzed black extracts from *M. edulis* shells really were melanin using infrared spectroscopy. The infrared spectra of the hydrolyzed extracts (Supplementary Figure S1B) revealed peaks at 3,300–3,500  $\text{cm}^{-1}$ , 1,600–1,670  $\text{cm}^{-1}$  and 1,250–1,465  $\text{cm}^{-1}$ , thus confirming that the extracts from the *M. edulis* shells were indeed melanin. Supplementary Figures S1C and S2 (available in [www.besjournal.com](http://www.besjournal.com)) show ultrastructural SEM images and XPS of extracted and T- and H-melanin.

### Analysis of Photothermal Conversion

We compared the photothermal conversion effects of *M. edulis* melanin hydrolyzed with concentrated HCl and various proteases (P-melanin). Figure 1A shows the relationship between the temperature of H-melanin and T-melanin, and the length of exposure to NIR irradiation (0.8 W, 808 nm). The temperature of hydrolyzed melanin changed roughly in three stages as follows. During the first 0–1 min, the temperature rapidly increased under near-infrared radiation, and immediately produced a thermal effect. The rate of the temperature increase gradually slowed over the next 1–6 min, then stabilized between 6–7 min. The temperature of T-melanin increased more rapidly, and peaked at 81.4 °C. The H-melanin peaked at 67.4 °C, and the P-melanin reached only 49 °C. These findings indicated that melanin can be photothermally converted by NIR irradiation to promote a local increase in temperature, thus exerting sterilization and inhibition effects, and that T-melanin was the most effective.

We assessed temperature changes of 25 to 200  $\mu\text{g}/\text{mL}$  of melanin to determine photothermal conversion at various concentrations (Figures 1B and 2A). Since the temperature of melanin suspended in water at 200  $\mu\text{g}/\text{mL}$  changed the most, we applied this concentration to calculate photothermal

conversion and to correspond with the doses in the antibacterial experiments *in vitro* and the biocompatibility assays *in vivo*. After irradiation for 5 min, the temperatures of the H-melanin and T-melanin suspensions and of pure water increased by 20.4 °C (Figure 1C), 23.2 °C (Figure 2B) and 11.2 °C, respectively.

Next, we measured the photothermal conversion efficiency ( $\eta$ ) of H-melanin and T-melanin as described<sup>[44]</sup>. The  $\eta$ ,  $t$ , and  $\vartheta$  values were calculated as:

$$\eta = \frac{hA\Delta T_{\max} - Q_s}{I(1 - 10^{-A_\lambda})}, \quad (1)$$

$$t = -\frac{\sum m_i C_{p,i}}{hA} \ln \vartheta, \quad (2)$$

$$\vartheta = \frac{\Delta T}{\Delta T_{\max}}, \quad (3)$$

where  $h$  is the heat transfer coefficient,  $A$  is the surface area of the container,  $\Delta T_{\max}$  is the temperature change in the melanin suspension at the maximum steady-state temperature,  $I$  is laser power,  $A_\lambda$  is absorbance of the melanin suspension at 808 nm,  $Q_s$  is the amount of heat associated with the light absorbance of the solvent (pure water; measured independently as 25.2 mW),  $\eta$  is photothermal conversion efficiency, and  $m$  and  $C$  are the mass and heat capacity of the solvent (water), respectively. According to Equation 1, and Figures 1E and 2D, the  $\eta$  values of H-melanin and T-melanin were 22.89% and 51.35%, respectively.

### Antibacterial Activity *in vitro*

We compared the bacteriostatic effects of T- and H-melanin against Gram-negative (*E. coli*) and positive (*S. aureus*) bacteria.

Figure 3A shows that the number of bacteria did not significantly change in the control group regardless of NIR irradiation. These findings indicated that NIR irradiation alone does not affect the normal growth of *E. coli* and *S. aureus*. After 15 min of incubation without irradiation, the numbers of *E. coli* and *S. aureus* did not significantly change in the T- and H-melanin groups compared with the controls, indicating that neither hydrolyzed melanin exerted bactericidal effects without NIR

irradiation. In contrast, the numbers of bacteria in the H- and T-melanin groups slightly and significantly decreased respectively, after 15 min of NIR radiation compared with none. These findings indicated H- and T-melanin was weakly, and more strongly bactericidal, respectively, against *E. coli* and *S. aureus*.

With NIR irradiation, the bacteriostatic rates of

H- and T-melanin against *E. coli* and *S. aureus* were 35.43% and 29.10% (Figure 3B), and 97.43% and 94.23%, respectively.

Changes in the morphology of individual *E. coli* and *S. aureus* cells after different treatments were assessed by TEM. Figure 3C shows that the bacteria in the control group appeared normal, with a complete membrane structure and a

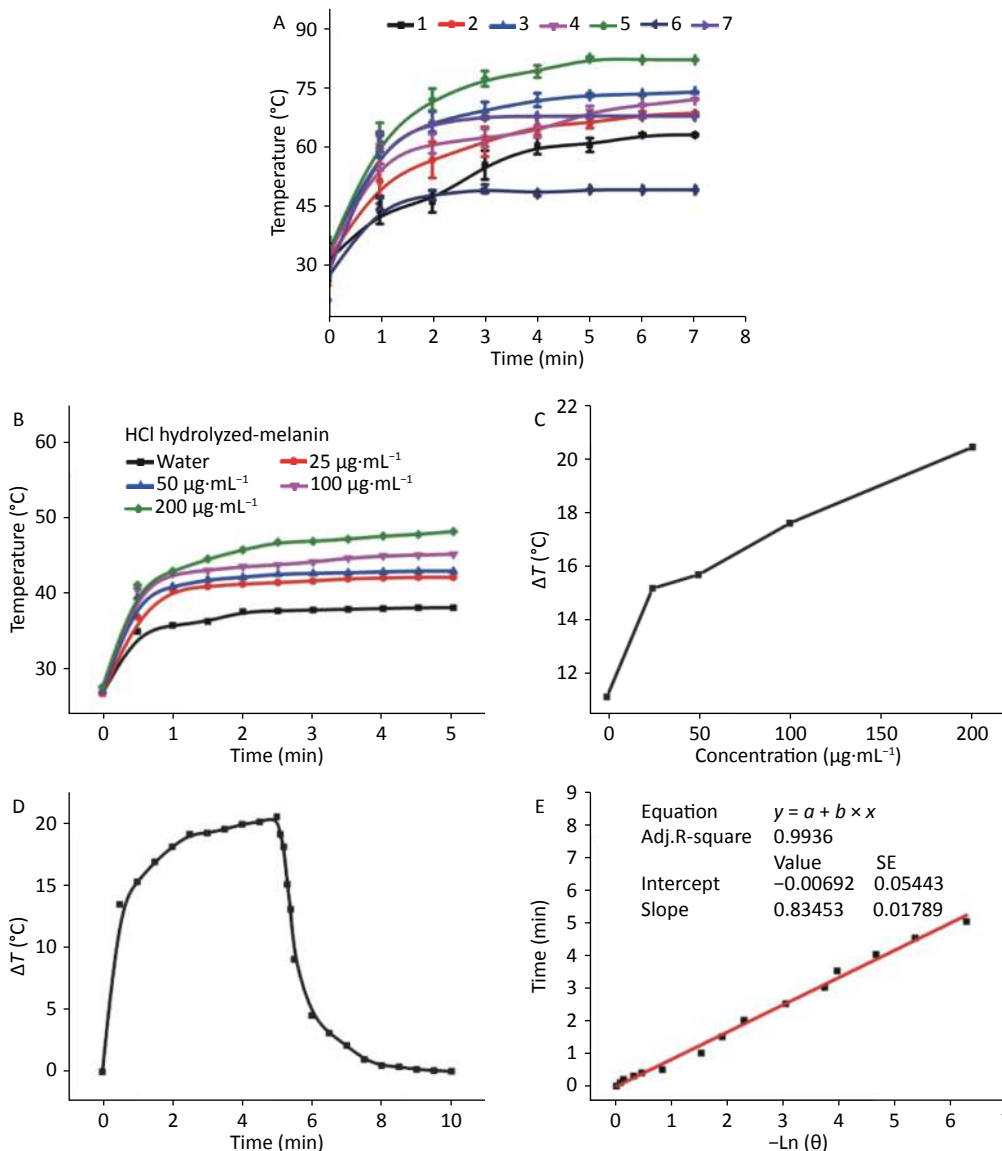


**Figure 1.** Photothermal conversional effects of hydrolyzed melanin. (A) Photothermal conversional effects of various concentrations of hydrolyzed melanin under NIR laser radiation at 0.8 W and 808 nm. Numbers 1 to 7 represent melanin hydrolyzed by pepsase, animal proteinase, neutral protease, alkaline protease, trypsin, compound protease, and HCl, respectively. (B) Increases in temperature of water and of aqueous suspensions of H-melanin according to duration of irradiation. (C) Temperature variations (Δ) in aqueous suspensions of H-melanin over 300 s. (D) Photothermal response of 200 μg/mL of aqueous H-melanin under NIR laser irradiation at 2 W and 808 nm for 5 min and then the laser was shut off. (E) Linear time data vs.  $-\ln(\theta)$  were acquired based on the cooling period shown in (C).

normal rod-like or spherical shape. The edges of *E. coli* and *S. aureus* cells exposed to NIR irradiation for 15 min and incubated with H-melanin were slightly broken, but the basic shape persisted. In contrast, the cell walls and membranes of these bacteria similarly exposed to NIR irradiation and incubated with T-melanin were completely ruptured, releasing the cytoplasm into the milieu (red arrow). These findings indicated that T-melanin together with NIR irradiation are bacteriostatic and can play a sterilizing role.

#### DAPI and PI Fluorescence-based Live/dead Assays

Bacterial viability after incubation with H- and T-melanin and exposure to NIR was determined using LIVE/DEAD BacLight kits (Thermo Fisher Scientific Inc.). Viable and dead bacteria are stained green and red, respectively.

Figure 4 shows that control *E. coli* and *S. aureus* incubated without H-melanin stained green with or without NIR irradiation, indicating that NIR alone

cannot kill these bacteria. Incubating the bacteria with H-melanin in the absence of NIR irradiation showed that H-melanin was not cytotoxic. Furthermore, NIR irradiation of the H-melanin group killed only a few cells, indicating a slight bactericidal effect against *E. coli* and *S. aureus*.

Green cells found after incubating these bacteria with T-melanin but without NIR exposure indicated that these bacteria remained viable. However, most cells exposed to T-melanin together with NIR irradiation were stained red, indicating that T-melanin exerted more powerful bactericidal and sterilization effects than H-melanin.

#### Wound Healing in vivo

Based on the antibacterial findings *in vitro*, we assessed the wound healing activities of H-melanin and T-melanin *in vivo*, individually. In brief, a rat model of bacterial infection was constructed by local infection with the resistant *S. aureus*. Thereafter, the infected rats were randomized as H-melanin, T-melanin, and control groups, separately (Figure 5).

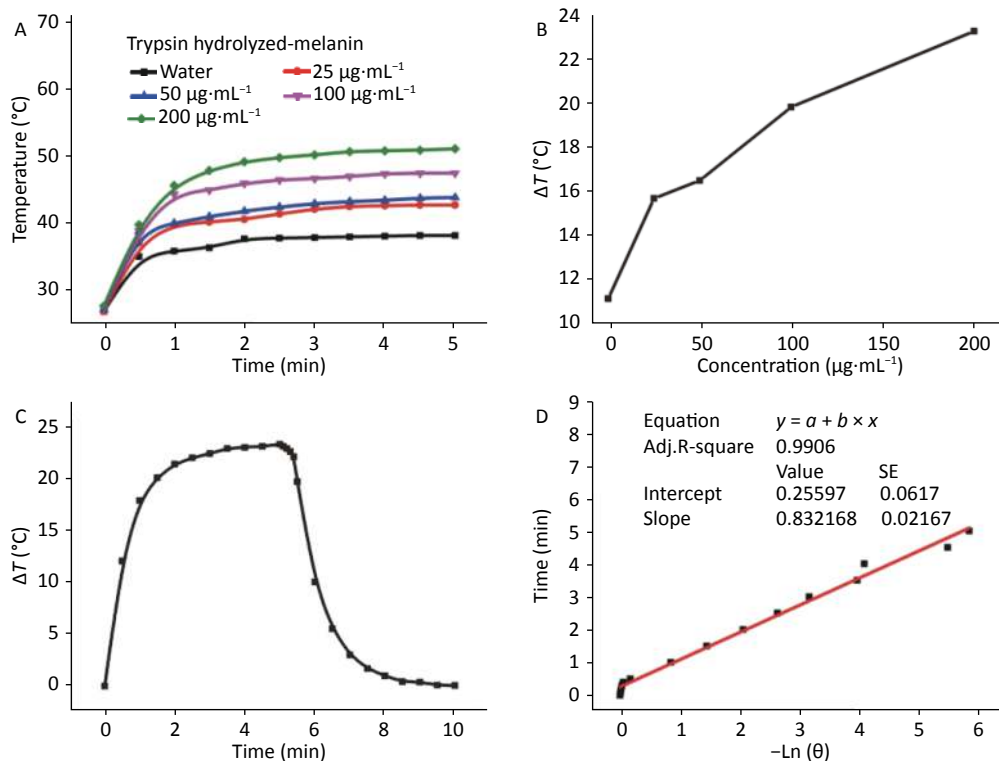


**Figure 2.** Photothermal responses of T-melanin. (A) Increases in temperature of water and aqueous T-melanin suspensions at various concentrations during irradiation for 5 min. (B) Temperature variations ( $\Delta T$ ) Temperature variations ( $\Delta$ ) in aqueous H-melanin suspension during 300 s. (C) Photothermal response of 200  $\mu\text{g}/\text{mL}$  of aqueous T-melanin under NIR laser irradiation at 2 W and 808 nm for 5 min and then later the laser was shut off. (D) Linear time data vs.  $-\ln\theta$  acquired based on cooling period shown in (C).

On the day 0, the drug-resistant *S. aureus* infected wounds in the three groups were of equal size. On the day 3, all three groups of wounds were healed to varying degrees. The T-melanin group with NIR+ had

the smallest wound area, followed by the H-melanin group, while the control group had the largest wound area. By day 6, the T-melanin group with NIR+ was basically healed, the healing effects were

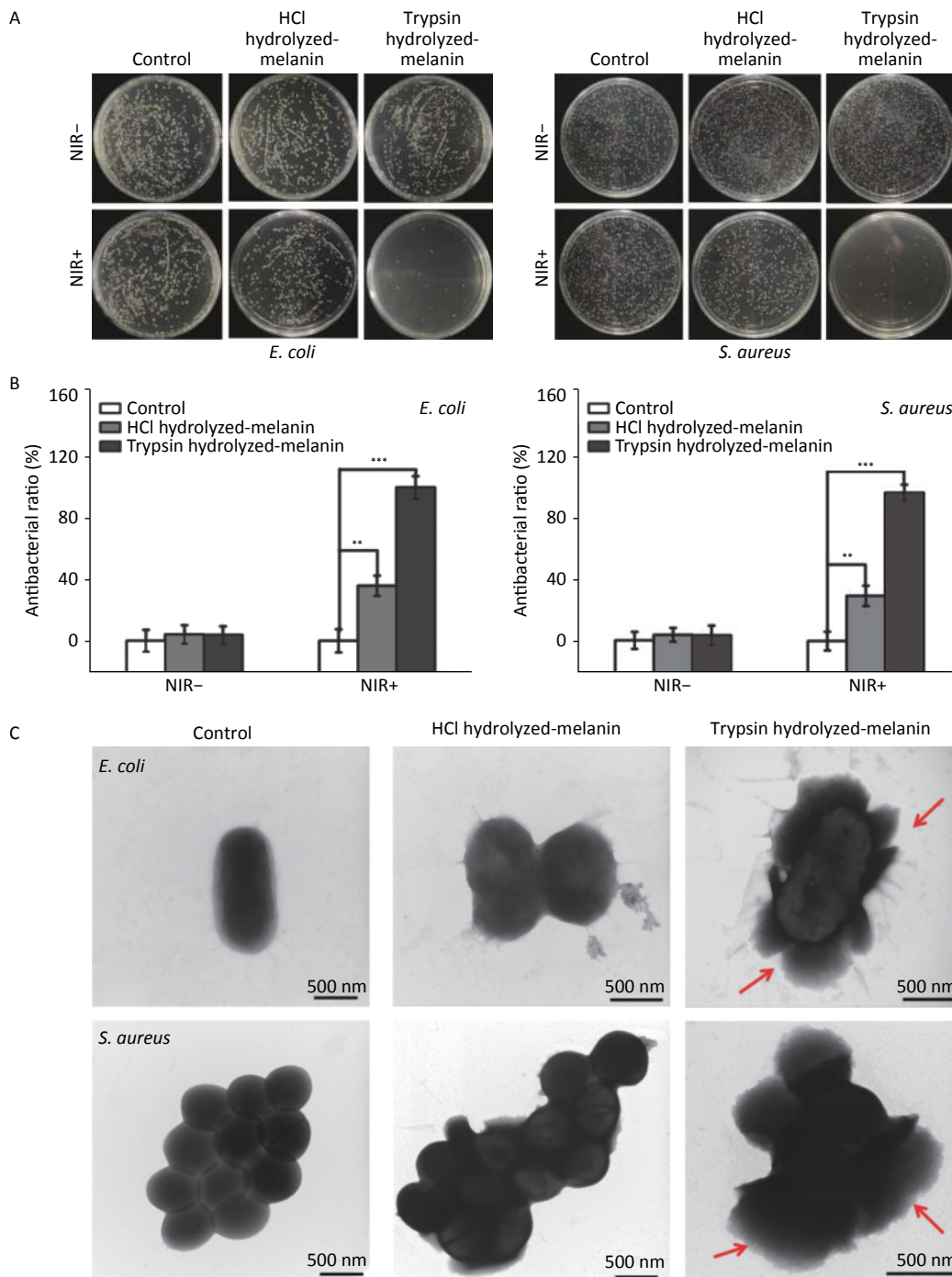


**Figure 3.** *Escherichia coli* (*E. coli*) and *Staphylococcus aureus* (*S. aureus*) incubated with H-melanin and T-melanin followed by NIR irradiation for 15 min. (A) Photographs show *E. coli* and *S. aureus* after incubation with melanin followed by NIR irradiation. (B) Antibacterial ratios against *E. coli* and *S. aureus*. Data are presented as means  $\pm$  SD ( $n = 3$ ;  $**P < 0.01$  and  $***P < 0.001$ ). (C) TEM images for *E. coli* and *S. aureus* incubated T-melanin and H-melanin. NIR-, without, and NIR+, with near infrared radiation.

significant compared with H-melanin and the control group.

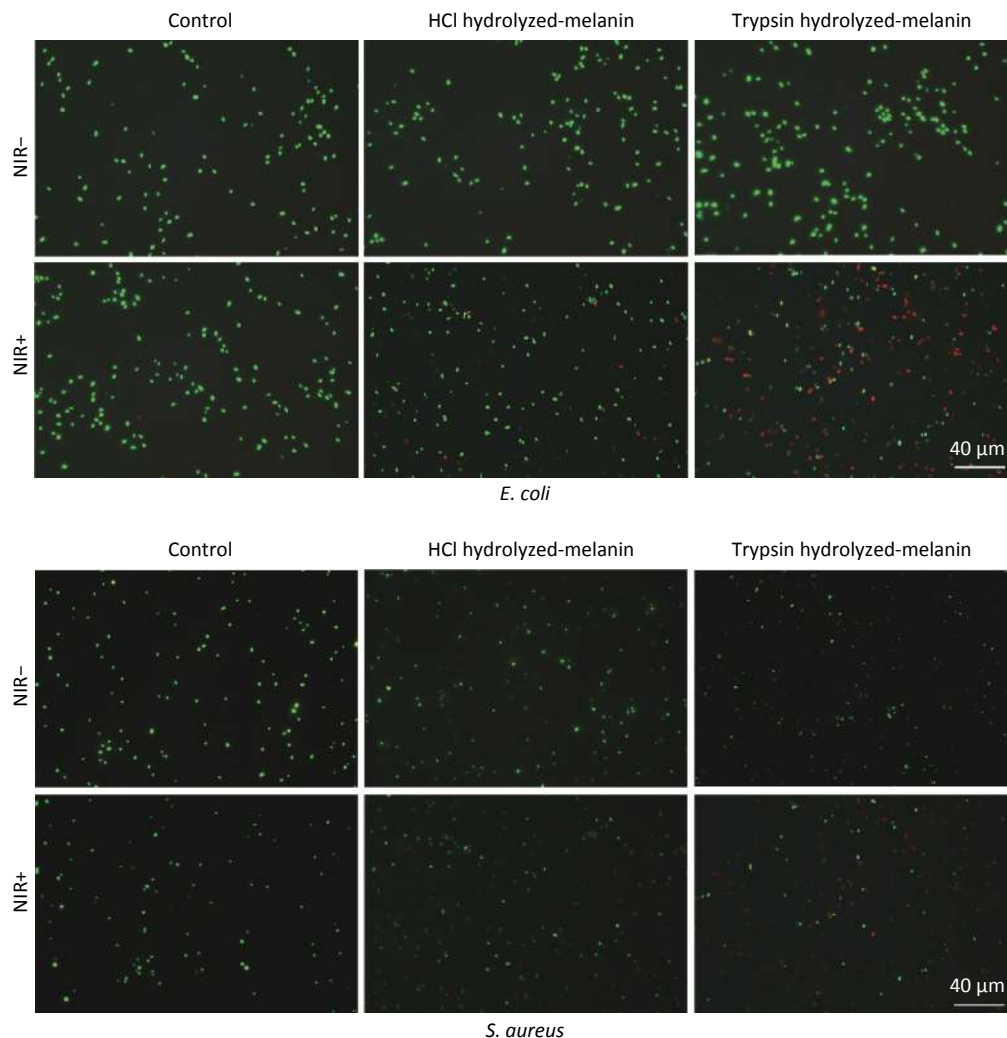
We quantified the wound healing process by comparing wound sizes on days 3 and 6 with that on day 0 (Figure 6A). The size of wounds significantly differed in the group treated with T-melanin and NIR radiation compared with the control on day 3 ( $P < 0.01$ ). The wounded area was significantly smaller on day 6 in the group treated with T-melanin and NIR radiation compared with the control ( $P < 0.05$ ) and the NIR-irradiated H-melanin group ( $P < 0.001$ ). These findings confirmed that the high temperature of NIR induced the maximal bactericidal effect of T-melanin against these methicillin-resistant bacteria.

Figure 6C shows infrared images of the temperature increase in wounds treated with melanin and NIR irradiation<sup>[45]</sup>. After 15 min of

irradiation at 2 W, local temperatures of the H- and T-melanin groups increased from 36.4 °C to 46.8 °C and 66.3 °C, respectively, indicating better photothermal conversion of T-melanin.

Wound tissues were harvested from each group of rats to further determine the abundance of *S. aureus* cells on days 0, 3, and 6 by counting CFU (Figure 6B). The number of bacterial colonies was the lowest on days 3 and 6 when treated with T-melanin and NIR irradiation compared with the control ( $P < 0.05$ ), followed by H-melanin with NIR irradiation. The wound healing capacity on day 6 was better for T- than H-melanin with NIR irradiation.

Wound tissues were stained with H&E on day 6 to evaluate wound healing. Neutrophils stain blue in infected tissues<sup>[46]</sup>. Figure 7 shows the histological findings of wounds in the control, H-



**Figure 4.** Representative fluorescence images of viability of *E. coli* and *S. aureus* cell incubated with T- or H-melanin and with or without NIR irradiation. NIR-, without, and NIR+, with near infrared radiation.

melanin and T-melanin groups without NIR. A blue arrow indicates inflammatory cells, suggesting serious infection of the wound. The skin at the surface of the wound surface is cracked and damaged (black arrow). In contrast, the ratio of inflammatory cells is very small in the wounds treated with T-melanin and NIR irradiation. This combination exerted the optimal healing effect as indicated by a smooth, complete skin surface (yellow arrow) and normal subcutaneous tissue structure (green arrows).

#### Cytotoxicity and *in vivo* Biocompatibility Assay

The above results indicated that T-melanin could offer a tremendous advantage for disinfecting wounds. Therefore, the biosafety of this nanomaterial should be considered.

We evaluated the cytotoxicity of T- and H-melanin *in vitro* using the MTT method, and tested relative survival by adding different volumes of

melanin suspension to L929 cells and HUVEC, respectively. Figure 8A shows that at melanin concentrations of 0–200  $\mu\text{g}/\text{mL}$ , the survival rates of these cells remained > 99%. Therefore, we considered that T- and H-melanin are safe and not cytotoxic *in vitro*.

We then assessed the cytotoxicity of H-melanin and T-melanin in mice *in vivo*. The main organ tissues of mice treated with melanin and stained with H&E showed no obvious organ abnormalities or inflammation, and their morphology and structure were similar to those of normal organs (Figure 8B). We also intravenously injected healthy Sprague-Dawley rats with aqueous H-melanin and T-melanin for 6 d, then assessed hepatorenal functions as blood biochemical values. These indexes did not significantly differ from those in untreated mice (Figure 8C). These results suggest that H-melanin and T-melanin are highly biocompatible, not toxic and do not elicit side effects *in vivo* and *in vitro*.

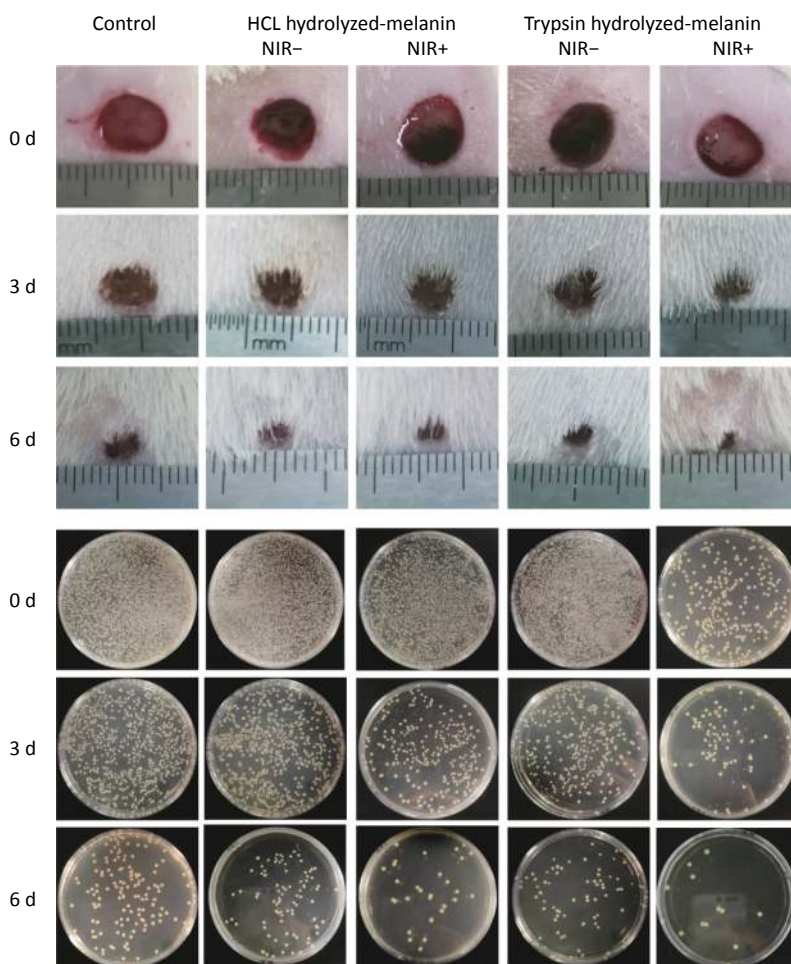


**Figure 5.** Wound tissues and bacterial colonies collected after treatment with melanin and NIR irradiation days 0, 3, and 6.

## CONCLUSIONS

We extracted natural melanin from *M. edulis* shells collected from Rizhao coast using HCl (acid hydrolysis) and trypsin (enzymolysis). We found that T-melanin killed methicillin-resistant Gram-positive *S. aureus* and Gram-negative *E. coli* bacteria *in vitro* by efficiently converting NIR

radiation into heat energy. We also evaluated the bactericidal ability of *M. edulis* melanin in a model of bacterial infection by locally infecting rats with drug-resistant *S. aureus*. The sterilization effects *in vivo* and *in vitro* were better for T-melanin than H-melanin. The results of MTT assays and physiological indices show that the NIR photothermal antibacterial method could provide

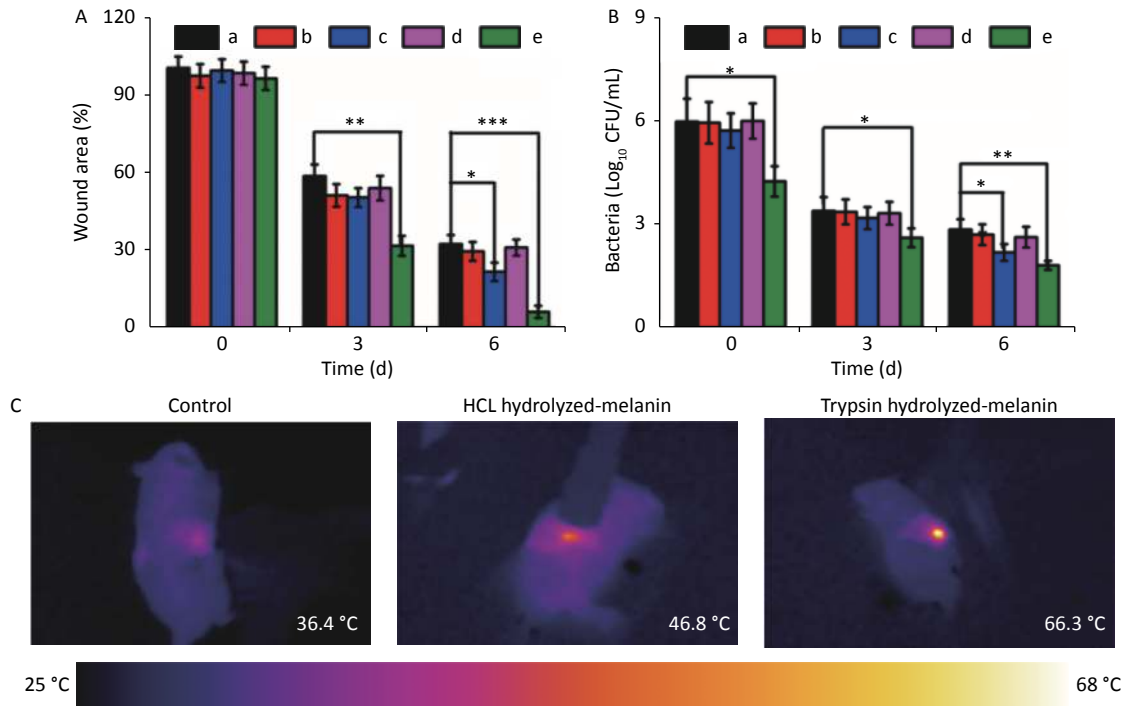


**Figure 6.** Wound sizes, bacterial CFU and thermal images. (A) Wound sizes in rats from different groups after various treatments. (B) Numbers of bacterial CFU in wound tissues on days 0, 3, and 6. Black, red, blue, magenta and green columns in A and B represent control, H-melanin and NIR-, H-melanin and NIR+, H-melanin and NIR-, and H-melanin and NIR+, respectively. (C) Thermal images of rats after various treatments. All data are shown as means  $\pm$  SD ( $n = 3$  rats per group). \* $P < 0.05$ , \*\* $P < 0.01$ , and \*\*\* $P < 0.001$ .

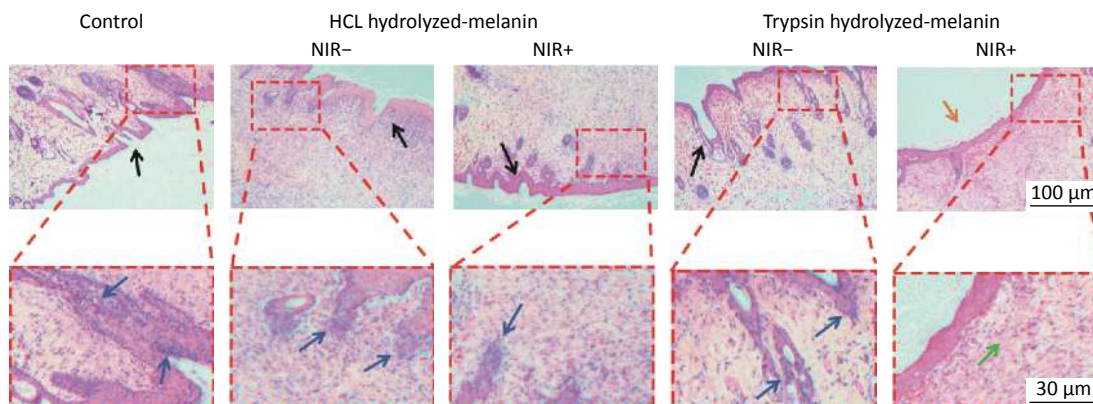


**Figure 7.** Status of skin tissue infection on day 6. Wound tissues were stained with H&E after various treatments. Scale bars indicate magnified boxed areas of tissue sections.

a novel solution to the problem of bacterial resistance. Further investigation is needed, because the bacteriostatic mechanism significantly differs from that of traditional antibiotics. Our findings might also stimulate new ideas for more effective utilization of marine resources and promote the application of natural pigments in healing and other diseases.

### CONFLICTS OF INTEREST

None of the authors has any conflicts to declare.

### AUTHORS' CONTRIBUTIONS

LIU Ya Mei, drafted the manuscript, conducted experiments, analyzed results. MA Wei Shuai, guided

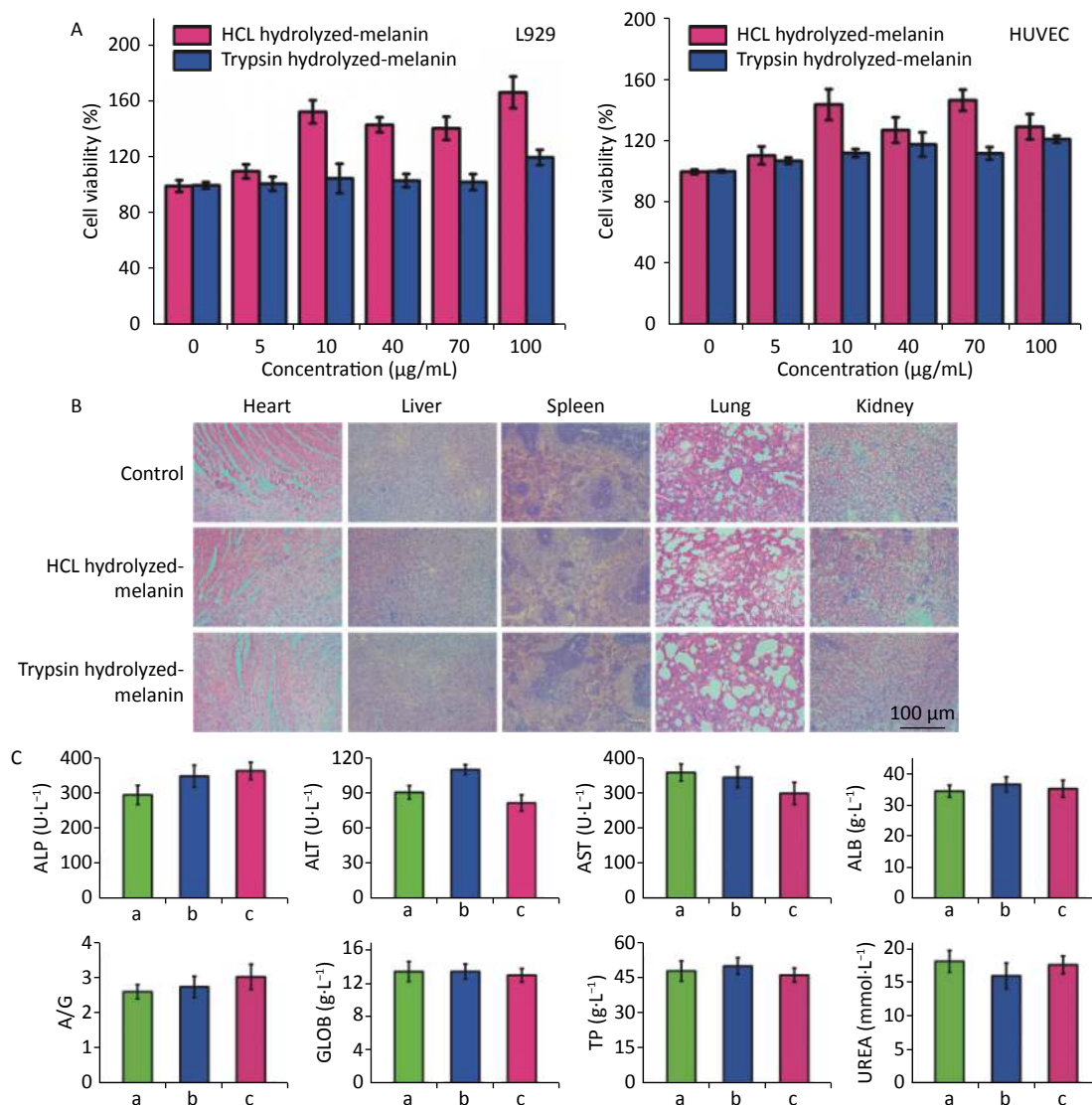


**Figure 8.** Cytotoxicity of H-melanin and T-melanin against L929 cells and HUVEC *in vitro* and in mice *in vivo*. Values are shown as means and standard deviations of three mice per group. (A) Cytotoxicity of H- and T-melanin against L929 cells and HUVEC *in vitro*. (B) Sections of heart, liver, spleen, lungs, and kidneys harvested from mice treated with or without (control; PBS) melanin (H&E stain). (C) Blood biochemical findings of mice under treated with (a) PBS, (b) H-melanin, (c) T-melanin. A/G, albumin-to-globulin ratio; ALB, albumin; ALP, alkaline phosphatase; ALT, alanine transaminase; AST, aspartate transaminase; GLOB, globulin; TP, total protein; UREA, urea nitrogen; HUVEC, human umbilical vein endothelial cells.

experimental methods, assisted with animal experiments. Wei Yu Xi, obtained *M. edulis* shells, guided melanin extraction and purification. Xu Yuan Hong, provided intellectual content, and revised the manuscript.

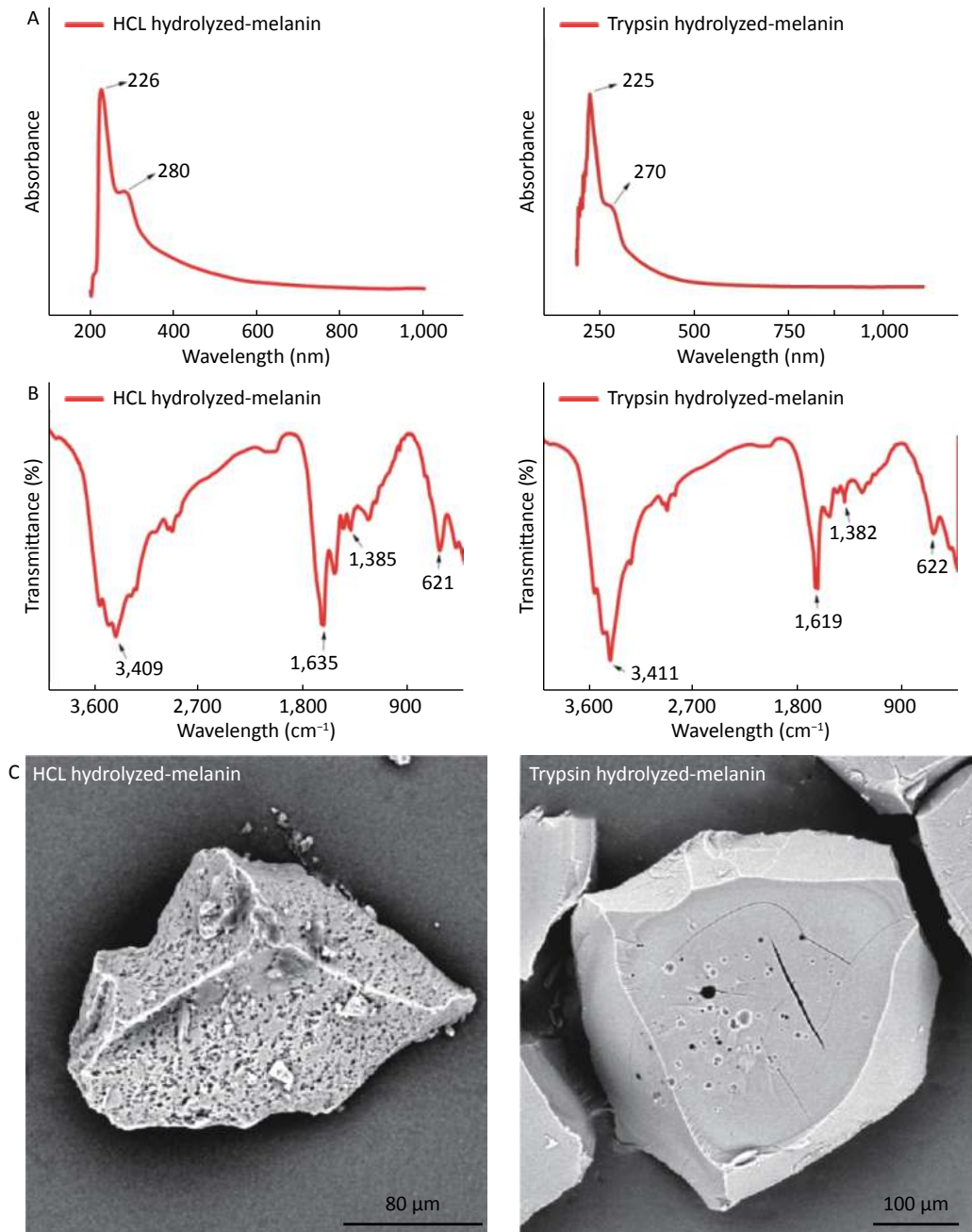
Received: March 6, 2020;

Accepted: May 21, 2020

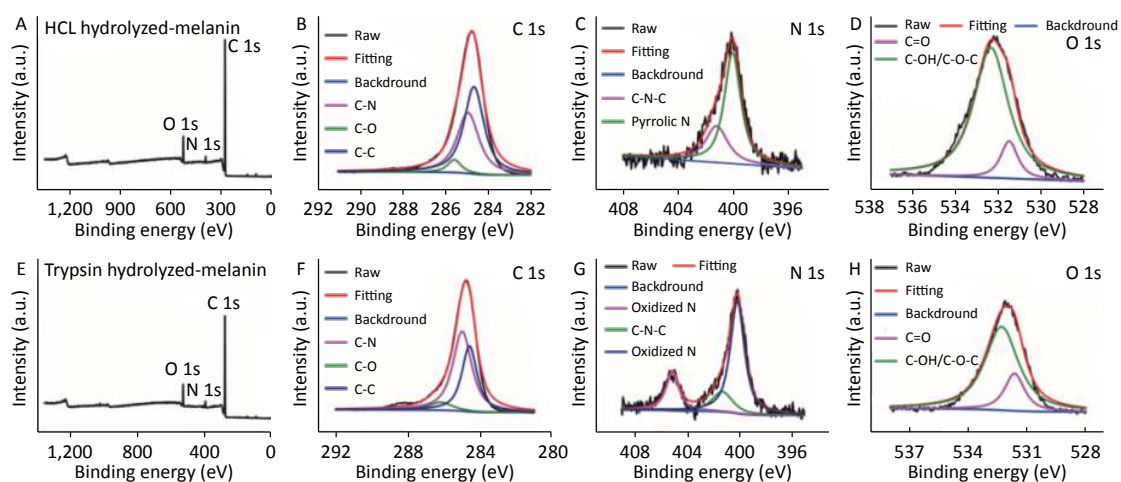
## REFERENCES

1. L Sheng, Y Lu, S Deng, et al. Transcription aptasensor: amplified, label-free and culture-independent detection of foodborne pathogens via light-up RNA aptamers. *Chem Commun*, 2019; 55, 10096–9.
2. P Li, YF Poon, W Li, et al. A polycationic antimicrobial and biocompatible hydrogel with microbe membrane suctioning ability. *Nat Mater*, 2011; 10, 149–56.
3. B Lu, F Lu, L Ran, et al. Imidazole-molecule-capped chitosan-gold nanocomposites with enhanced antimicrobial activity for treating biofilm-related infections. *J Colloid Interface Sci*, 2018; 531, 269–81.
4. H Maaoui, R Jijie, GH Pan, et al. A 980 nm driven photothermal ablation of virulent and antibiotic resistant Gram-positive and Gram-negative bacteria strains using Prussian blue nanoparticles. *Colloid Interface Sci*, 2016; 480, 63–8.
5. Y Zhao, Z Chen, Y Chen, et al. Synergy of nonantibiotic drugs and pyrimidinethiol on gold nanoparticles against superbugs. *J Am Chem Soc*, 2013; 135, 12940–3.
6. A Kassem, GM Ayoub, L Malaeb. Antibacterial activity of chitosan nano-composites and carbon nanotubes: a review. *Sci Total Environ*, 2019; 668, 566–76.
7. HL Shane, E Lukomska, ML Kasha, et al. Topical application of the quaternary ammonium compound didecylmethylammonium chloride activates type 2 innate lymphoid cells and initiates a mixed-type allergic response. *Toxicol Sci*, 2019; 168, 508–18.
8. Y Li, W Zhang, J Niu, et al. Mechanism of photogenerated reactive oxygen species and correlation with the antibacterial properties of engineered metal-oxide nanoparticles. *ACS Nano*, 2012; 6, 5164–73.
9. B Peng, YB Su, H Li, et al. Peng. Exogenous alanine and/or glucose plus kanamycin kills antibiotic-resistant bacteria. *Cell Metab*, 2015; 21, 249–62.
10. X Zhao, H Wu, B Guo, et al. Antibacterial anti-oxidant electroactive injectable hydrogel as self-healing wound dressing with hemostasis and adhesiveness for cutaneous wound healing. *Biomaterials*, 2017; 122, 34–47.
11. KA Brogden. Antimicrobial peptides: pore formers or metabolic inhibitors in bacteria? *Nat Rev Microbiol*, 2005; 3, 238–50.
12. JE Bean, DR Alves, M Laabei, et al. Triggered release of bacteriophage K from agarose/hyaluronan hydrogel matrixes by *Staphylococcus aureus* virulence factors. *Chem Mater*, 2014; 26, 7201–8.
13. LJ Zhang, CF Guerrero-Juarez, T Hata, et al. Dermal adipocytes protect against invasive *Staphylococcus aureus* skin infection. *Science*, 2015; 347, 67.
14. L Li, Y Liu, P Hao, et al. PEDOT nanocomposites mediated dual-modal photodynamic and photothermal targeted sterilization in both NIR I and II window. *Biomaterials*, 2015; 41, 132–40.
15. B Hu, N Wang, L Han, et al. Magnetic nanohybrids loaded with bimetal core-shell-shell nanorods for bacteria capture, separation, and near-infrared photothermal treatment. *Chem Eur J*, 2015; 21, 6582–9.
16. F Solano. Melanin and melanin-related polymers as materials with biomedical and biotechnological applications—cuttlefish ink and mussel foot proteins as inspired biomolecules. *Int J Mol Sci*, 2017; 18, 1561.
17. A Elsaesser, CV Howard. Toxicology of nanoparticles. *Adv Drug Delivery Rev*, 2012; 64, 129–37.
18. V Manirethan, K Raval, R Rajan, et al. Data on the removal of heavy metals from aqueous solution by adsorption using melanin nanopigment obtained from marine source: *Pseudomonas stutzeri*. *Data Brief*, 2018; 20, 178–89.
19. KP Watts, RG Fairchild, DN Slatkin, et al. Melanin content of hamster tissues, human tissues, and various melanomas. *Cancer Res*, 1981; 41, 467–72.
20. Y Liu, K Ai, J Liu, et al. Dopamine-melanin colloidal nanospheres: an efficient near-infrared photothermal therapeutic agent for in vivo cancer therapy. *Adv Mater*, 2013; 25, 1353–9.
21. M Araújo, R Viveiros, TR Correia, et al. Natural melanin: a potential pH-responsive drug release device. *Int J Pharm*, 2014; 469, 140–5.
22. CJ Bettinger, JP Bruggeman, A Misra, et al. Biocompatibility of biodegradable semiconducting melanin films for nerve tissue engineering. *Biomaterials*, 2009; 30, 3050–7.
23. KY Ju, Y Lee, S Lee, et al. Bioinspired polymerization of dopamine to generate melanin-like nanoparticles having an excellent free-radical-scavenging property. *Biomacromolecules*, 2011; 12, 625–32.
24. JM Menter, AM Patta, TD Hollins, et al. Photoprotection of mammalian acid-soluble collagen by cuttlefish sepia melanin in vitro. *Photochem Photobiol*, 1998; 68, 532–7.
25. LHLXD Yahui, LJSNZ Liyuan. Ultrastructure and antioxidative activity of melanin from cuttlefish. *Inst Food Sci Technol*, 2012; 10, 62–6.
26. X Guo, S Chen, Y Hu, et al. Preparation of water-soluble melanin from squid ink using ultrasound-assisted degradation and its anti-oxidant activity. *J Food Sci Technol*, 2014; 51, 3680–90.
27. S Chen, J Xu, C Xue, et al. Sequence determination of a non-sulfated glycosaminoglycan-like polysaccharide from melanin-free ink of the squid *Ommastrephes bartrami* by negative-ion electrospray tandem mass spectrometry and NMR spectroscopy. *Glycoconjugate J*, 2008; 25, 481–92.
28. I to. Reexamination of the structure of eumelanin. *Acta Gen Subj*, 1986; 883, 155–61.
29. Jr Liebscher, R Mrówczyński, HA Scheidt, et al. Structure of polydopamine: a never-ending story? *Langmuir*, 2013; 29, 10539–48.
30. S Ito, K Wakamatsu, M d'Ischia, et al. Structure of melanins. Wiley Online Library pp, 2011; 167–85.
31. U Grienke, J Silke, D Tasdemir. Bioactive compounds from marine mussels and their effects on human health. *Food Chem*, 2014; 142, 48–60.
32. B Wang, L Li, CF Chi, et al. Purification and characterisation of a novel antioxidant peptide derived from blue mussel (*Mytilus edulis*) protein hydrolysate. *Food Chem*, 2013; 138, 1713–9.
33. A Naik, M Hayes. Bioprocessing of mussel by-products for value added ingredients. *Trends Food Sci Technol*, 2019; 92, 111–21.
34. L Huang, Y Niu, R Li, et al. VOx quantum dots with multienzyme-mimic activities and the application in constructing a three-dimensional (3D) coordinate system for accurate discrimination of the hydrogen peroxide over a broad concentration range. *Anal Chem*, 2019; 91, 5753–61.

35. Y Chen, MY Xie, SP Nie, et al. Purification composition analysis and antioxidant activity of a polysaccharide from the fruiting bodies of *Ganoderma atrum*. *Food Chem*, 2008; 107, 231–41.
36. CR Prakash, S Raja, Synthesis. characterization and *in vitro* antimicrobial activity of some novel 5-substituted schiff and mannich base of isatin derivatives. *J Saudi Chem Soc*, 2013; 17, 337–44.
37. C Ge, R Wu, Y Chong, et al. Synthesis of Pt hollow nanodendrites with enhanced peroxidase-like activity against bacterial infections: implication for wound healing. *Adv Funct Mater*, 2018; 28, 1801484.
38. L Hang, Y Niu, G Xu, et al. Generation of vanadium oxide quantum dots with distinct fluorescent property and antibacterial activity *via* a room-temperature agitation strategy. *Chem Nano Mat*, 2018; 4, 1048–53.
39. L Yuan, Y Niu, R Li, et al. Molybdenum oxide quantum dots prepared via one-step stirring strategy and applications as fluorescent probes for pyrophosphate sensing and efficient antibacterial materials. *J. Mater. Chem B*, 2018; 6, 3240–5.
40. Y Li, W Ma, J Sun, et al. Electrochemical generation of Fe<sub>3</sub>C/N-doped graphitic carbon nanozyme for efficient wound healing *in vivo*. *Carbon*, 2019; 159, 149–60.
41. JR Nakkala, R Mata, SR Sadras. Green synthesized nano silver: Synthesis, physicochemical profiling, antibacterial, anticancer activities and biological *in vivo* toxicity. *J Colloid Interface Sci*, 2017; 499, 33–45.
42. AA Bell, MH Wheeler. Biosynthesis and functions of fungal melanins. *Annu Rev Phytopathol*, 1986; 24, 411–51.
43. P Selvakumar, S Rajasekar, K Periasamy, et al. Isolation and characterization of melanin pigment from *Pleurotus cystidiosus* (telomorph of *Antromyces macrocarpa*). *World J Microbiol Biotechnol*, 2008; 24, 2125–31.
44. DK Roper, W Ahn, M Hoepfner. Microscale heat transfer transduced by surface plasmon resonant gold nanoparticles. *J Phy Chem C*, 2007; 111, 3636–41.
45. S Wu, A Li, X Zhao, et al. Silica coated gold-silver nanocages as photothermal antibacterial agents for combined anti-infective therapy. *ACS Appl Mater Interfaces*, 2019; 11, 17177–83.
46. Y Xiang, C Mao, X Liu, et al. Rapid and superior bacteria killing of carbon quantum dots/ZnO decorated injectable folic acid-conjugated PDA hydrogel through dual-light triggered ROS and membrane permeability. *Small*, 2019; 15, 1900322.



**Supplementary Figure S1.** (A) UV absorption spectra of HCl hydrolyzed-melanin and trypsin hydrolyzed-melanin. (B) FTIR spectra of HCl hydrolyzed-melanin and trypsin hydrolyzed-melanin. (C) SEM images of HCl hydrolyzed-melanin and trypsin hydrolyzed-melanin.



**Supplementary Figure S2.** (A) XPS survey spectrum of HCl hydrolyzed-melanin. (B) XPS C1S spectrum of HCl hydrolyzed-melanin. (C) XPS N1s spectrum of HCl hydrolyzed-melanin. (D) XPS O1s spectrum of HCl hydrolyzed-melanin. (E) XPS survey spectrum of trypsin hydrolyzed-melanin. (F) XPS C1S spectrum of trypsin hydrolyzed-melanin. (G) XPS N1s spectrum of trypsin hydrolyzed-melanin. (H) XPS O1s spectrum of trypsin hydrolyzed-melanin.